Thermally Induced Wind Passing from Plain to Basin over a Mountain Range

FUJIO KIMURA AND TSUNEO KUWAGATA

Geophysical Institute, Tohoku University, Sendai, Japan

(Manuscript received 23 September 1992, in final form 11 March 1993)

ABSTRACT

A new concept of a thermally induced local circulation is presented by numerical and observational studies. This wind system transports a low-level air mass from a plain to a basin, passing over a mountain ridge. The characteristics of the wind system are investigated using two- and three-dimensional numerical models.

Upslope winds develop over the mountain slopes surrounding the basin until late afternoon. These winds are composed of separate individual circulations both inside and outside the basin. The atmospheric temperature in the boundary layer within the basin becomes higher than that outside, so that the surface pressure becomes lower at the bottom of the basin than that outside.

At dusk, the thermal forcing due to the surface heat flux decreases, weakening the upslope winds, and then a plain-to-basin wind develops over the mountain ridges due to the pressure difference formed in the daytime. The plain-to-basin circulation is generated when the altitude of the mountain range is almost equal to or less than the maximum mixing height developed over the plain. Higher mountain ranges act as potential barriers of the circulation.

The plain-to-basin winds are most remarkable when the horizontal scale of the basin is less than approximately 100 km and the height of the mountain range is approximately equal to the maximum mixing height. For larger horizontal scales, the velocity of the plain-to-basin wind is weaker.

Two observational examples of the plain-to-basin wind are presented. The first example is known as a part of the system that carries pollutants from the Tokyo area to the Saku Basin and develops over a mountain pass in the evening. The other wind system develops during the afternoon over a valley that connects a basin to a plain. This wind system is observed for the first time in the present work.

1. Introduction

The daytime heating rate in the lower atmosphere at the bottom of a basin is greater than that over a plain on a clear, calm day (Kondo et al. 1989). The accumulated warmer air at the bottom of the basin induces a surface pressure depression during the daytime (Kuwagata et al. 1990a,b; Kuwagata and Sumioka 1991).

This fact can be explained by the concept of the topographic amplification factor (TAF) discussed by Whiteman (1990). According to this concept, the sensible heat from the ground surface in a basin warms only the atmosphere in the basin whose volume is smaller than that over a plain. Thus, the temperature of the lower atmosphere in the basin increases more than that over the plain. The topographical effect on the heating rate can be quantitatively represented by the value of the TAF, which is the ratio of the atmospheric volume in the basin to that of the flat plain.

On the other hand, Kondo et al. (1989) suggested that the larger heating rate over the basin bottom is attributed to local subsidence heating, which occurs in the compensating current of the thermally induced upslope flow.

Corresponding author address: Dr. Fujio Kimura, Geophysical Institute, Tohoku University, Aramaki, Aoba-Ku, Sendai 980, Japan.

The daytime pressure difference between the basin and plain may generate a surface wind that flows from the plain to the basin, although the separating mountain range may act as a barrier to suppress such a wind system. This wind system should therefore depend on the topographic features and on atmospheric conditions.

Basins in the Japanese islands often record high levels of air pollution at night, presumed to have been transported from large plains outside of the basin area (Kurita et al. 1990). The wind system mentioned above could be an important component in the transportation mechanism, creating a general tendency for basins to attract pollutants emitted from areas outside the basin.

Kuwagata et al. (1990b) estimated the mean surface heat flux in basins for clear, calm days from the profile of potential temperature, calculated from the diurnal variation in the surface pressure and neglecting heat advection from regions outside the basin. If the above-mentioned plain-to-basin wind exists on clear, calm days, it may affect the heat budget in the basin.

In the present study, characteristics of the plain-to-basin wind generated by the pressure difference are investigated with the use of a two-dimensional local circulation model. Three-dimensional effects of the topography are also investigated by a three-dimensional version of the model. Finally, several examples of the

wind system discussed in the present work are shown, including the wind systems that transport pollutants as mentioned above.

2. The numerical model

The model is based upon the two-dimensional Boussinesq equations using the hydrostatic assumption. The model includes a turbulent closure model in the boundary layer and a prognostic equation for the surface temperature. The governing equations and the numerical scheme of the model are the same as for the model developed by Kikuchi et al. (1981) and modified by Kimura and Arakawa (1983). The equations can be written as

$$\frac{\partial hu}{\partial t} + \frac{\partial huu}{\partial x} + \frac{\partial huw^*}{\partial z^*} = -h\Theta \frac{\partial \pi'}{\partial x} + gh \frac{\theta'}{\Theta} \frac{z_T - z^*}{z_T} \frac{\partial z_G}{\partial x} + \frac{\partial}{\partial x}\left(hK_H \frac{\partial u}{\partial x}\right) + \frac{z_T^2}{h} \frac{\partial}{\partial z^*}\left(K_m \frac{\partial u}{\partial z^*}\right), \quad (1)$$

$$\frac{\partial h\theta'}{\partial t} + \frac{\partial hu\theta'}{\partial x} + \frac{\partial hw^*\theta'}{\partial z^*} = \frac{\partial}{\partial x}\left(hK_H \frac{\partial \theta'}{\partial x}\right) + \frac{z_T^2}{h} \frac{\partial}{\partial z^*}\left(K_h \frac{\partial \theta'}{\partial z^*}\right), \quad (2)$$

$$\frac{\partial}{\partial x} hu + \frac{\partial}{\partial z^*} hw^* = 0, \quad (3)$$

and

$$\frac{\partial \pi'}{\partial z^*} = \frac{h}{z_T} \frac{g\theta'}{\Theta^2}. \quad (4)$$

Here, z^* is the terrain-following vertical coordinate defined as

$$z^* = z_T \frac{z - z_G}{h}, \quad h = z_T - z_G, \quad (5)$$

in which z_T and z_G are the levels at the top and ground surface of the model atmosphere, respectively.

The two-dimensional version of the model will be mainly applied here. In section 4, however, some results of the three-dimensional version of the same model will be shown for a discussion of the three-dimensional effects of topography.

In the two-dimensional model, two mountain ridges are separated by a narrow valley. Figure 1 shows the assumed topography and grid points of the model. The shape of the topography is constructed from two cycles of sine function with a 60-km wavelength and two flat regions with 40-km width each. This figure shows the model topography with the mountain height of 1500 m; the heights and the horizontal distance between the mountains are varied in the model simulations. Since

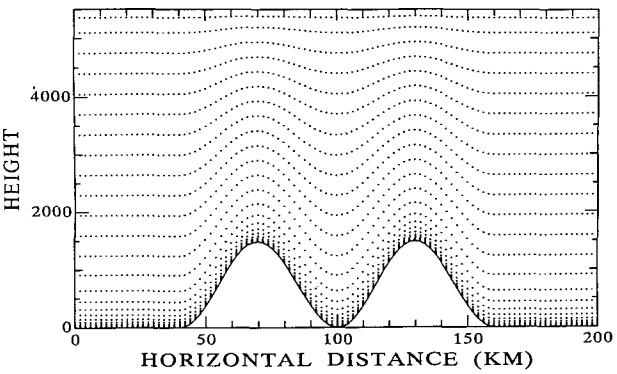

FIG. 1. A cross section showing the assumed topography and grid points of the model. Note that the mountain heights as well as the horizontal distance between the mountains are varied in the model simulations.

periodic lateral boundary conditions are applied, the two flat regions near both side lateral boundaries actually create one very wide valley. The wide valley simulates a plain, while the narrow valley between the mountain ranges acts as a basin. The grid domain consists of 100 grid points, located with a uniform horizontal interval, and 25 layers, with a smaller interval in the lower layers. The top boundary is controlled by the wave radiation condition given by Klemp and Durran (1983) and Bougeault (1983), in order to avoid reflections of gravity waves generated by the local circulations in the lower layers.

The vertical diffusion coefficient is estimated by the turbulent closure model (at level 2) developed by Mellor and Yamada (1974). Below the lowest vertical grid point ($z^* = 10$ m), a constant flux layer is assumed to estimate the sensible and latent heat fluxes.

The force–restore method (Bhumralkar 1975) is employed to obtain the surface temperature. The surface soil parameters such as heat capacity c, heat conductivity k, and evaporation efficiency β are assigned the values listed in Table 1.

Calm and clear synoptic conditions are assumed for the initial and boundary conditions. Other assumptions are also summarized in Table 1.

3. Plain-to-basin wind simulated by the two-dimensional model

To display the simulated wind system passing over the mountain range, the distribution of particles acting as tracers is calculated using the method of a random walk model (Kimura and Yoshikawa 1988). The particles are emitted at the surface-level point shown by the arrow in Fig. 2a, at the rate of one particle per minute and are then transported by the two components of the wind velocity supplied by the numerical model with the random vertical motion estimated from the vertical diffusivity, while lateral diffusion is neglected.

TABLE 1. Parameters used in the two-dimensional model.

Heat capacity	2.0×10^6 J m^{-3} K^{-1}
Conductivity	1.0 W m^{-1} K^{-1}
Evaporation efficiency	0.3
Albedo	0.12
Initial vertical temperature gradient	0.004 K m^{-1}
Relative humidity	70%
Initial sea level air temperature	290 K
Surface roughness parameter	0.05 m
Interfacial Stanton number	8.0
Solar elevation	summer solstice at 35°N

At 1200 LT (Fig. 2a), the particles have been diffused vertically up to the mixing height, about 1 km high, and are moved slowly toward the mountain range by the weak upslope wind. The high-density air column at the head of the polluted air mass was previously formed during the morning when the wind velocity was close to zero. By 1500 LT (Fig. 2b), the particles have been transported to the summit of the mountain range, while still being diffused vertically within the mixed layer.

The tracer particles were transported upward through the mixing height over the mountaintop by 1800 LT (Fig. 2c) but were still limited to the area outside the basin. At 1900 and 2000 LT (Figs. 2d,e), however, the particles penetrated into the basin, forming a few-hundred-meter-thick layer. The particles reached the bottom of the basin at about 2100 LT (Fig. 2f), although they never crossed the center of the basin due to the symmetry of the flow.

Figure 3 shows streamlines [(a)–(c)] and contours of potential temperature [(d)–(f)] at 1200, 1800, and 2000 LT, respectively. At 1200 LT, upslope winds are well developed on all slopes of the mountain, forming four independent circulations as shown in the figures. The mixed layer developed inside the basin accumu-

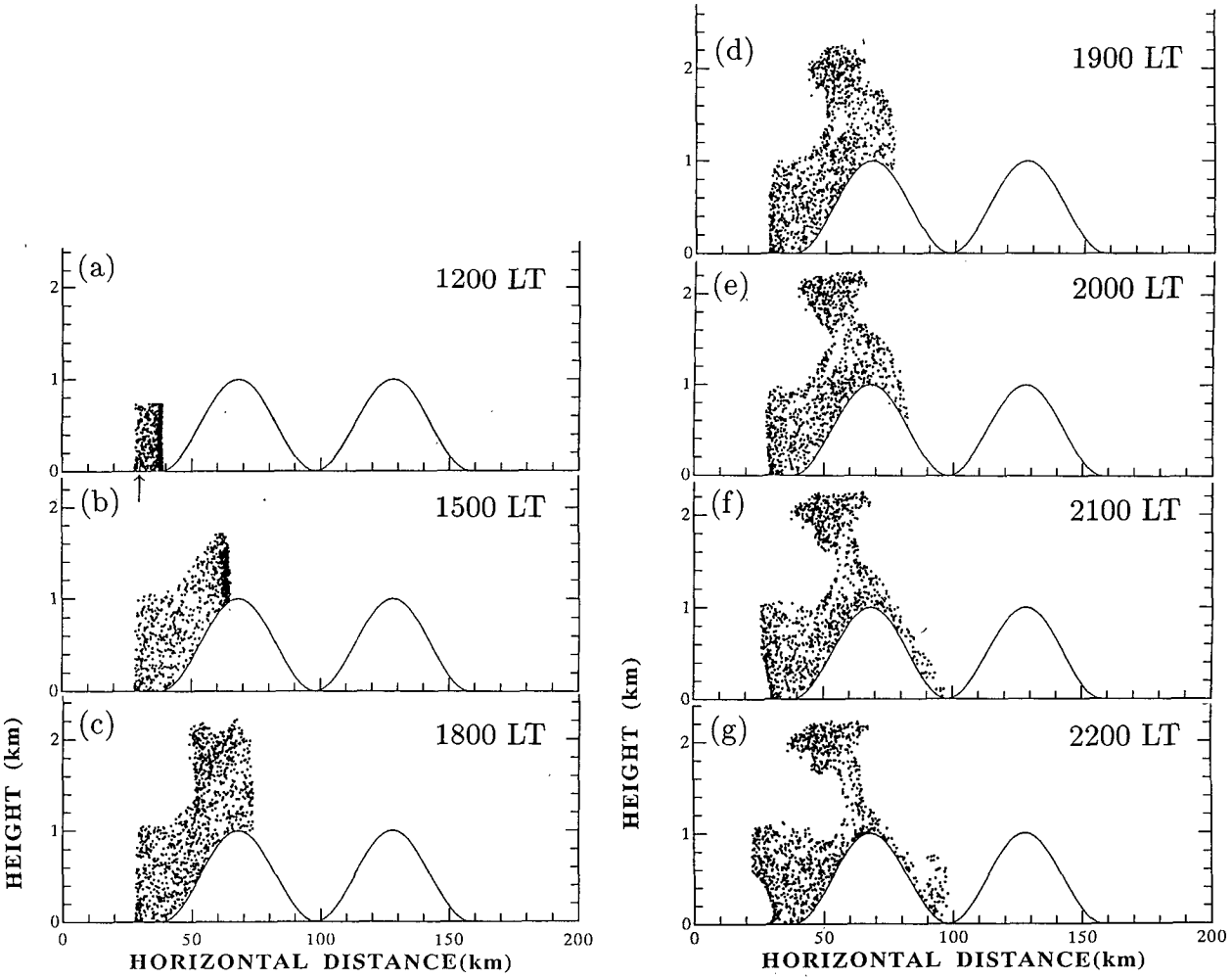

FIG. 2. Time series (a)–(g) of distribution of tracer particles produced by a random walk model using the wind and turbulence results of the two-dimensional model for the control case (the height of the mountain range is 1 km and the width of the basin, peak to peak is 60 km).

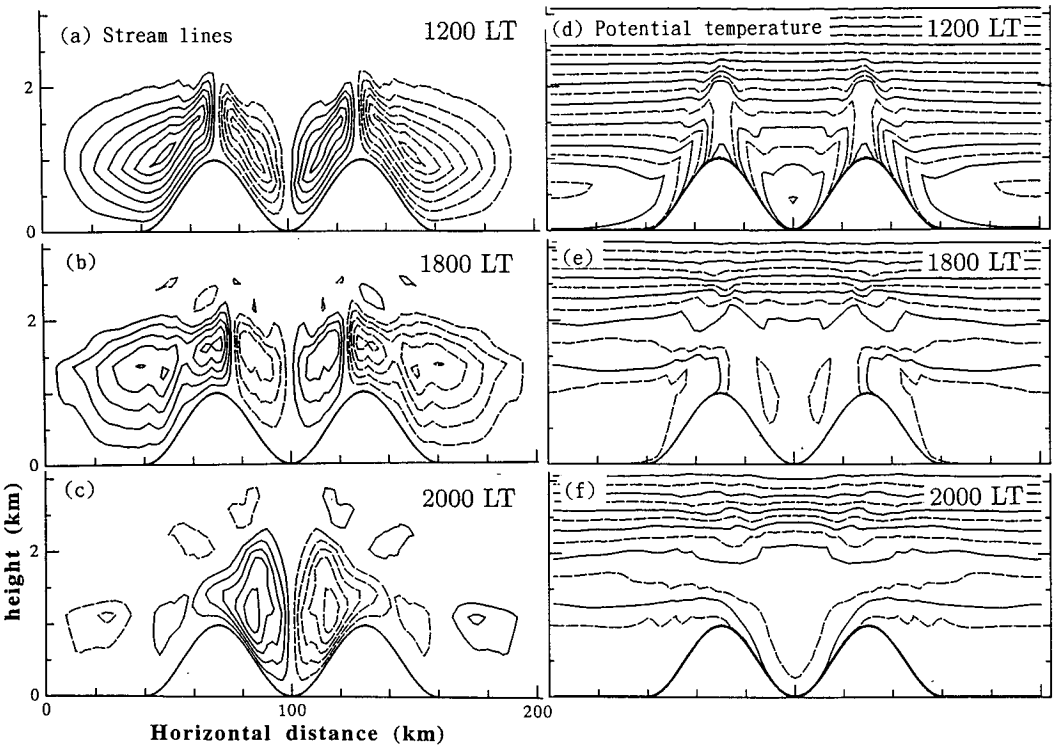

FIG. 3. Streamlines (a)–(c) and contours of potential temperature (d)–(f) at 1200, 1800, and 2000 LT, respectively (control case). The interval of the streamlines is 250 $m^2 s^{-1}$, while the solid line of potential temperature is 1 K. The dashed streamlines indicate clockwise circulations.

lated more sensible heat than that over the plain, creating a larger surface depression inside the basin.

At dusk (1800 LT: Figs. 3b and 3e), the thermal forcing by surface heat flux has become weak and the upslope winds begin to decay. New circulations are then generated over the mountain ranges with low-level winds flowing from the plain to the valley. By about 2000 LT (see streamlines in Fig. 3c), the surface wind inside the basin has changed to downslope direction. Figure 3f (potential temperature at 2000 LT) shows that relatively cooler air previously located over the plain has just penetrated to the bottom of the basin as a gravity current (cf. Fig. 3e). This means that the plain-to-valley winds have reached the bottom of the basin. These winds are responsible for the transport of cooler air from the plain to the basin and contribute to the reduction of the temperature difference between the plain and basin. Figure 4 shows the temporal distribution of velocities at 150 m above the ground surface at the median points of the plain- and basin-side slopes of the left-hand mountain range shown in Fig. 1. Positive velocities denote an upslope wind in the figure. During the daytime, upslope winds are almost symmetrically developed over both slopes of the mountain range.

After dusk, a strong downslope wind is initially found over the basin slope. A weaker downslope wind then appears over the plain slope. The stronger wind is a part of the plain-to-basin wind, which has a much thicker extent and stronger velocity than the normal downslope wind generated by the cooling of the slope surface. The weaker wind over the plain slope is part of the normal downslope wind. When it first begins to flow, its thickness and velocity tend to be larger than those after midnight. One reason for this may be the

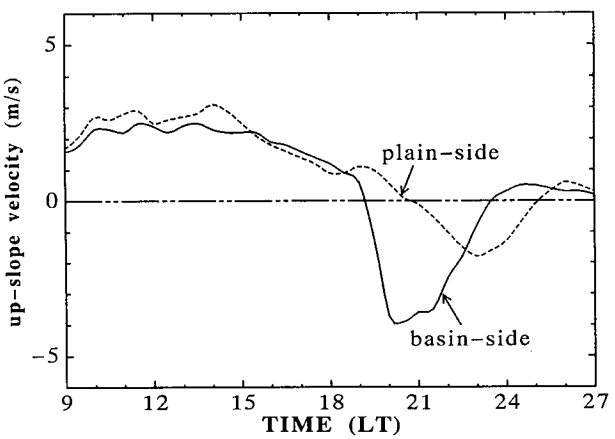

FIG. 4. The temporal history of the upslope wind speed at 150 m above ground surface at the median points of plain (dashed line) and basin (solid line) slopes of the left-hand mountain range (the control case).

rebound of the internal gravity waves generated by the upslope wind in the daytime.

After midnight, upslope winds appear over both slopes and the wind system again becomes symmetric. These upslope winds are counterflows of the normal thermally induced downslope winds, which are found below 150 m in the quasi-stationary state.

Figure 5 shows velocities over the basin-side median point mentioned above but for basin widths of 30, 60, and 120 km. For a 30-km width, the plain-to-basin wind begins to develop most rapidly just after sunset. In this case, the maximum wind speed is higher than that for a 60-km width but it terminates earlier (2200 LT). On the other hand, when the basin width is 120 km, the plain-to-basin wind begins to flow more slowly with a lower maximum velocity, but it remains past midnight. The slower development is caused by the smaller horizontal pressure gradient.

The plain-to-basin wind also depends on the height of the mountain range. Figure 6 is the same as Fig. 5, but for various heights of the mountain range. The plain-to-basin wind is most prominent for a mountain range height of 1 km. If the mountain height is lower than 1 km, the wind is weak. On the other hand, the circulation terminates earlier for cases of higher mountain ranges. If the mountain height is over 2 km, the plain-to-basin wind is no longer significant (not shown).

Figure 7 shows potential temperature distribution at 2000 LT for a mountain height of 2 km. Since the height of the mixing layer is much lower than the mountain range, the cold air within the mixed layer over the plain cannot cross the barrier mountain.

The plain-to-basin circulation is generated when the altitude of the mountain range is almost the same as or less than the maximum height of the mixed layer developed over the plain. In this case, the air mass needs only trivial additional energy to move over the mountain range. However, if the mountain range is much higher than the mixed layer, the air mass needs a huge amount of additional energy to be transported up and over the mountain barriers.

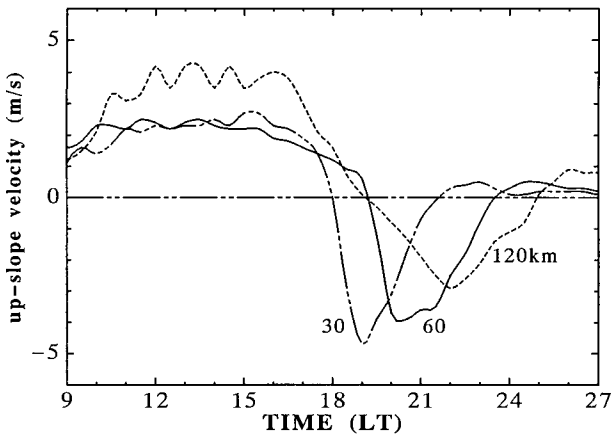

FIG. 5. The temporal distribution of the upslope wind speed at the basin-side median point for various basin widths: 30 km (double dotted line), 60 km (solid line; control case), and 120 km (dashed line). The height of the mountain range was maintained at 1 km.

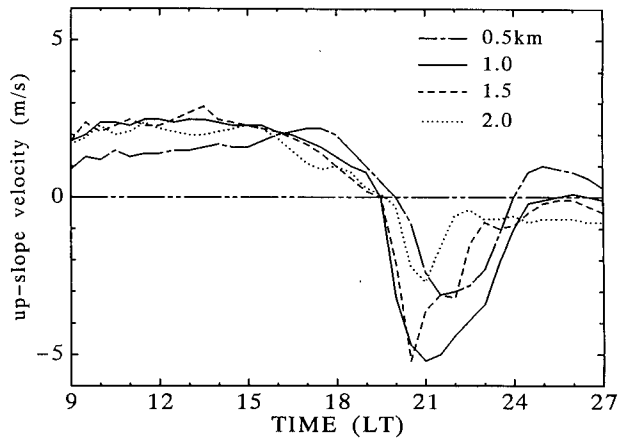

FIG. 6. The same as Fig. 5 but for various heights of the mountain range: 2 km (dotted line), 1.5 km (dashed line), 1 km (solid line), and 0.5 km (dot–dash line). Width of the basin is 60 km.

4. The three-dimensional plain-to-basin wind

In the previous section, two-dimensional simulations were carried out to clarify the wind system that developed around a basin between two mountain ranges having the same height. However, the heights of the surrounding mountain ranges of real basins vary widely, and some mountain passes with low elevations may exist. The basin may even contain some valleys that connect the basin to a plain or other basins acting as channels.

The plain-to-basin wind can be expected to be enhanced over the mountain pass or the channellike valley because of the lower barrier effect. Using a three-dimensional version of the model, the enhancement due to the channellike valley will be investigated.

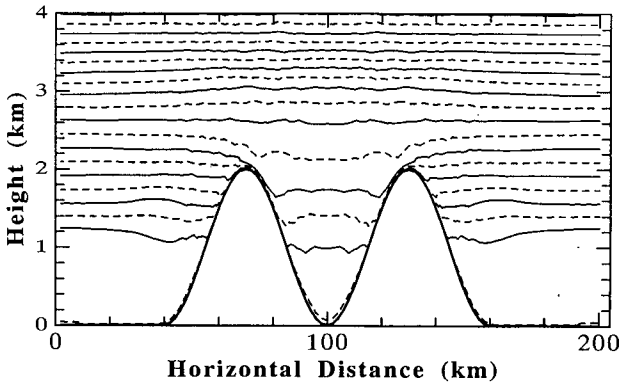

FIG. 7. Potential temperature distribution at 2000 LT for a mountain height of 2 km. The contour interval for the solid lines is 1 K.

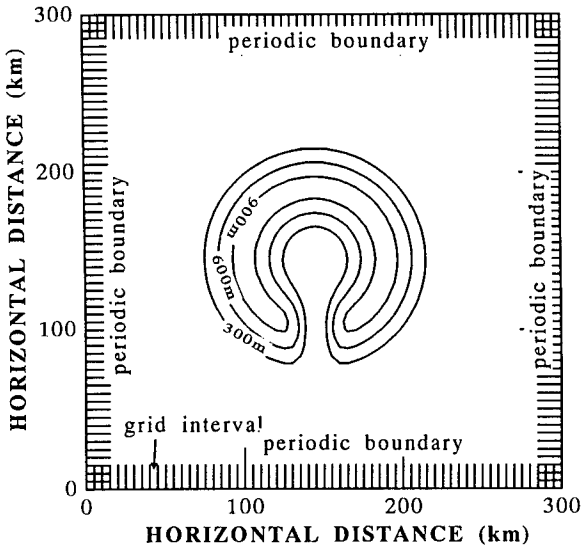

FIG. 8. A contour map of the topography for three-dimensional simulation. Grid interval is 5 km.

Figure 8 shows the model topography, which has a basin surrounded by a circular mountain range whose radius is 45 km with a peak height of 1 km. The mountain range has a gap of 20-km width and zero minimum elevation, which simulates a narrow valley connecting the basin and plain. The grid interval is 5 km, and the domain is covered by 50 × 50 grid points.

At 1200 LT (Fig. 9a), upslope winds are well developed and converge sharply along the mountain ridge. At 1500 LT (Fig. 9b), the convergence line has penetrated inside the basin, but only for a trivial distance. It can be seen that the wind system from the plain to the basin has already appeared in the valley.

By 1800 LT (Fig. 9c), the upslope winds have become weak and the convergence line over the ridge has become unclear. However, the plain-to-basin wind through the valley becomes stronger, covering all of the basin.

This three-dimensional simulation demonstrates that the plain-to-basin wind is more prominent with an earlier onset when a mountain pass or a valley connects the basin and plain.

5. Observed wind systems from plain to basin

a. Kanto Plain to Saku Basin

The long-range transport of air pollutants from coastal areas (for example, the Kanto Plain) to the mountainous inland regions (the Saku Basin) is often observed on clear summer days under conditions of a synoptic-scale high pressure system. Figure 11 shows the topography around the Saku Basin, the area indicated by the box marked with the letter A in Fig. 10.

Figure 12 was taken from Kurita et al. (1990) and shows the movement of zones of high concentrations of O_X(oxidant) + NO_X(nitrogen oxides) in the Kanto Plain–Saku Basin region. The numbers shown within each zone denote the time of the observation in hours (JST).

The pollutants were emitted from the Tokyo area and located in the northwestern part of the Kanto Plain during the late afternoon hours. They were then transported inland by the large-scale sea breeze. In the early evening, the polluted air mass has penetrated into the Saku Basin moving over the Usui Pass.

As shown in Fig. 11, the mountain pass (Usui Pass) has an altitude of 956 m above sea level (ASL), the typical elevation of the Kanto Plain is below 100 m ASL, while the bottom of the inland Saku Basin is between 400 and 500 m ASL.

Figures 13a–f show the diurnal variation of the observed horizontal wind vectors in the vertical plane along the transport route of the pollutants, which can

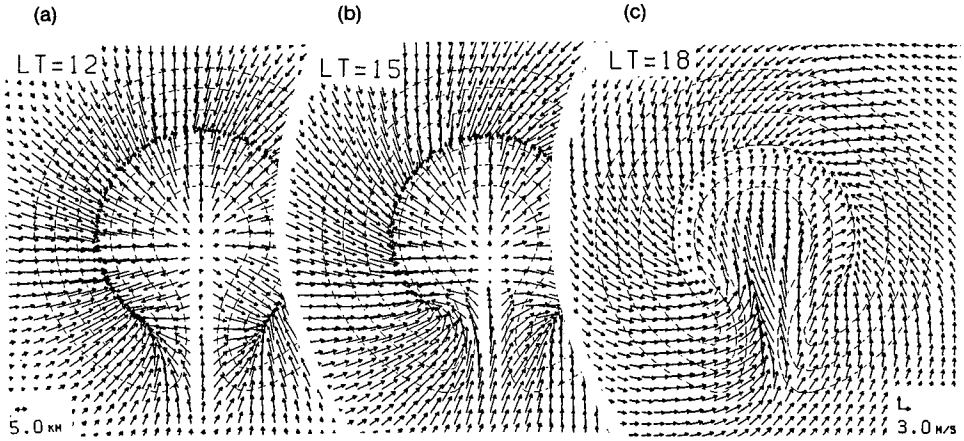

FIG. 9. Wind velocity vectors at 10 m above the ground surface calculated by the three-dimensional numerical model for various times: (a) 1200 LT, (b) 1500 LT, and (c) 1800 LT. The grid interval is 5 km. Each figure shows only the part of the domain that is of interest. The dashed lines are contours of elevation with a 300-m interval.

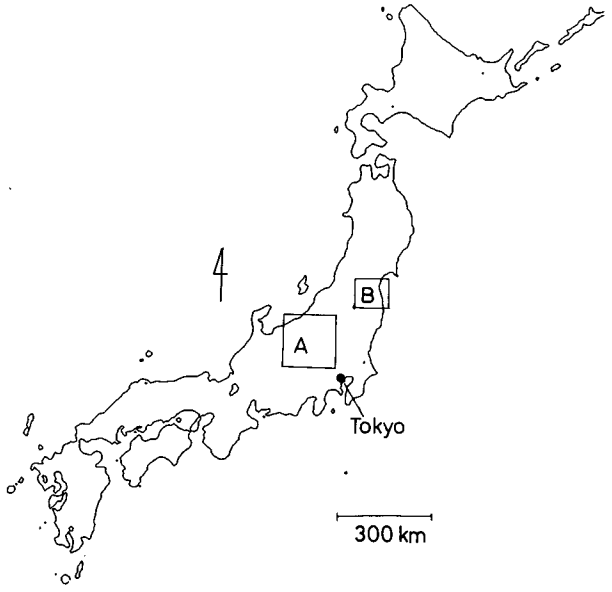

FIG. 10. A map of the Japanese islands showing the location of Saku and Fukushima basins, indicated by the boxes marked A and B, respectively.

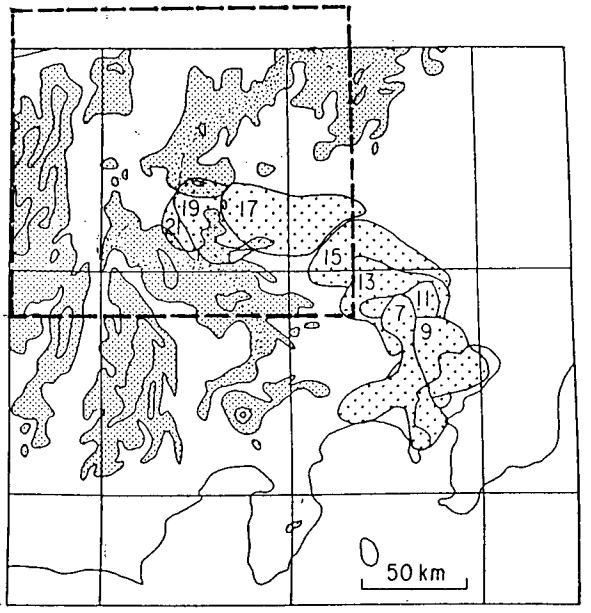

FIG. 12. Movement of the zones of high concentrations of O_X + NO_X, on 29 July 1983, after Kurita et al. (1990). The box of broken lines indicates the area shown by Fig. 11.

be roughly determined in Fig. 12. Kurita et al. (1990) suggested the following mechanism for the long-range pollution transport.

1) After sunrise, the sea breeze develops in the coastal area and a valley wind appears in the inland mountainous region (Fig. 13a).

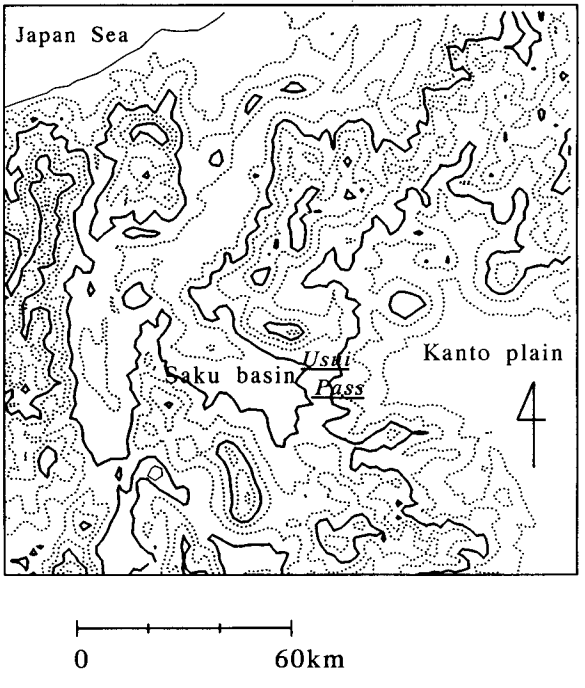

FIG. 11. The topography in the vicinity of the Saku Basin. The dotted counter lines are for every 300 m MSL, while the thick lines are every 900 m.

2) Around afternoon, the local sea breeze develops into the extended sea breeze, penetrating far inland to the area of the plain (Figs. 13b,c). The differential heating between the mountainous region and the plain generates a significantly strong thermal low in the mountainous region during the afternoon.

3) In the late afternoon the local wind systems, consisting of the sea breeze and valley wind, merge into the large-scale wind system flowing toward the thermal low.

4) The thermally induced large-scale wind intrudes into the inland basin, moving over the mountain pass (Fig. 13d).

5) During the nighttime, after the thermal low weakens, the intruding air is further transported down along the valley of the inland basin by the mountain winds, which also act as gravity currents (Fig. 13e,f).

Kurita et al. (1990) also stressed that the thermal low that occurs over a wide area of the mountainous region in central Japan is important in the transport of pollutants to the Saku Basin. The mechanism they suggested is still a conceptual idea.

The results of the present study explain how the polluted air penetrates into the basin along the Usui Pass during the evening. Figure 13 shows that the thermally induced wind begins intruding into the inland basin around 1600–1700 JST, and weakens around 2400 JST. These times are nearly the same as the plain-to-basin wind predicted by the two-dimensional numerical model.

The results of the present work suggest that the heat low does not cover the entire mountainous region but exists over individual basins in the mountainous region.

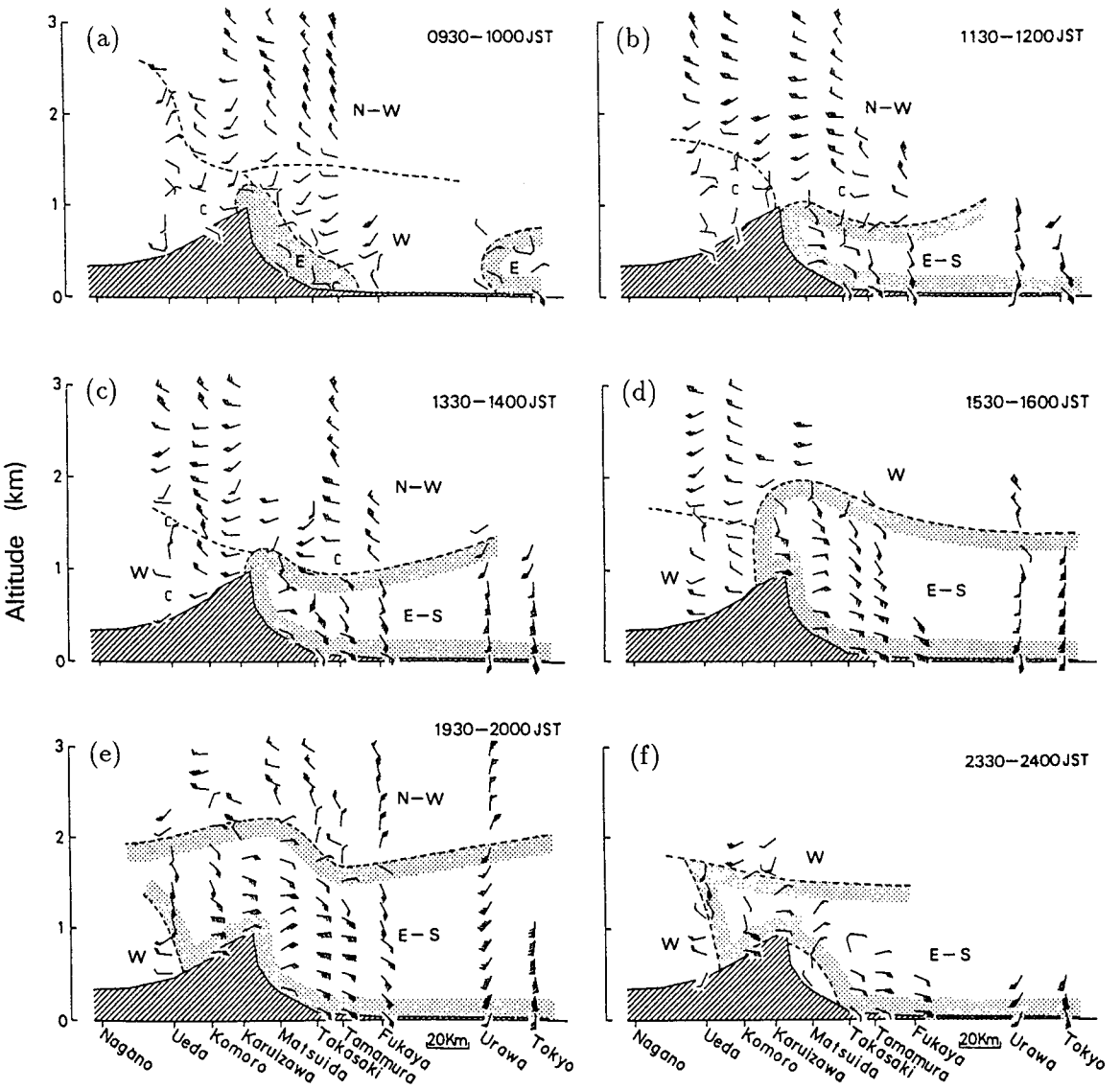

FIG. 13. The diurnal variation of the horizontal wind vectors in the vertical plane along the long-range transport route on 29 July 1983, after Kurita et al. (1990).

The intensities of the small heat lows over the basins may differ from each other.

The pollutants are transported from the plain to the basin by the plain-to-basin wind that develops during the evening hours. However, the mechanism for the transport of pollutants from the Tokyo area to the northwestern part of the Kanto Plain can still be explained by the extended sea breeze, which is thermally affected by the entire area of the mountainous region as Kurita et al. (1990) suggested.

b. Sendai Plain to the Fukushima Basin

The topography of Fukushima Basin is shown in Fig. 14, the location of which is indicated by the letter B in Fig. 10. In the northern part of the basin, a narrow valley exists that connects the basin to the Sendai Plain.

Pilot balloon observations were carried out at Yanagawa, indicated by the letter *Y* in Fig. 14, during 5–8 June 1990. Yanagawa is located inside the basin and near the entrance of the narrow valley. Clear skies and calm winds prevailed on both 5 and 8 June, since the Japan mainland was under the influence of an anticyclone.

Figures 15a and 15b show time–height cross sections of the horizontal wind velocity vectors observed on 5 and 8 June, respectively. On 5 June, southerly or southwesterly winds prevailed throughout the day at the 1000-m level. At 1400 JST, northerly winds suddenly appeared in the lowest 500 m. The northerly wind remained until about 2100 JST, although its

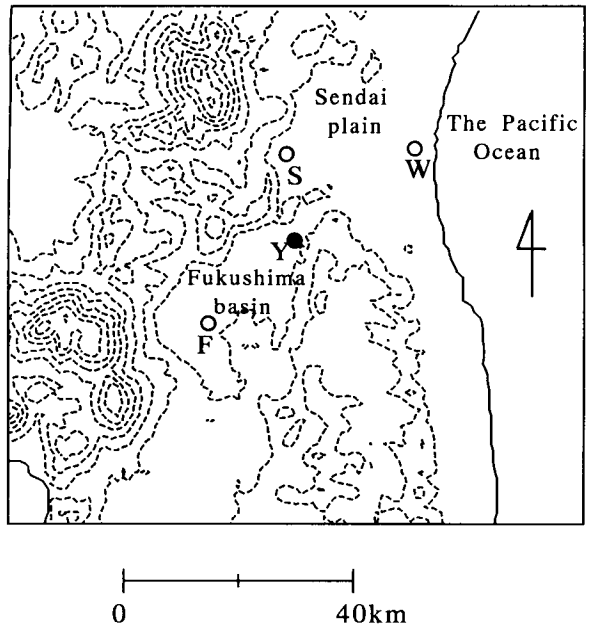

FIG. 14. The topography in the vicinity of the Fukushima Basin. The contour lines are every 200 m MSL.

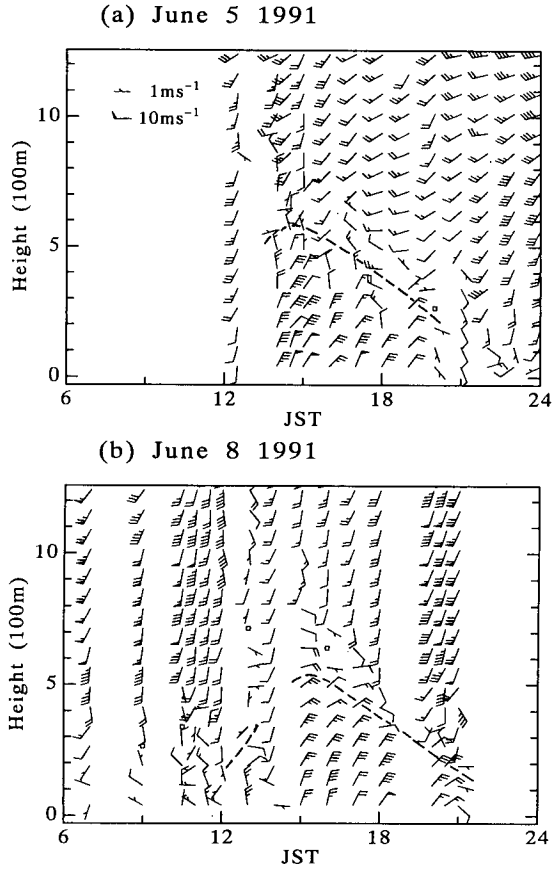

FIG. 15. The time–height cross section of the observed wind at the station *Y* shown in Fig. 14 on the (a) 5 June and (b) 8 June 1990. Dashed lines indicate the level speculated to be the top boundary of the plain-to-basin wind.

depth became more shallow with time. The diurnal variation of the wind profile on 8 June (Fig. 15b) was similar to that on 5 June.

The maximum velocities on 5 and 8 June were about 11 and 9 m s^{-1}, respectively, and appeared at the 100–200-m level. The prevailing wind direction was north-northwest, which agrees with the direction toward the Sendai Plain through the valley.

The surface wind velocity observed at 1500 JST 8 June by the AMeDAS of the Japan Meteorological Agency is shown in Fig. 16. The Sendai Plain was dominated by the sea breeze, whose direction was mainly southwest, while the Fukushima Basin recorded southerly winds. Only at the two stations near the narrow valley that connects the Sendai Plain to the Fukushima Basin were northerly winds observed. These northerly winds could well be the plain-to-basin wind.

Figure 17 shows the diurnal variation of the surface temperature observed on 8 June at the four stations lettered *W, S, Y,* and *F,* as shown in Fig. 14. The arrows in Fig. 17 denote the time when the surface wind direction significantly changed.

At station *W,* the sea breeze appears at about 0900 JST, suppressing any increase in temperature during the entire day. At stations *Y* and *F,* which are located in the Fukushima Basin, the temperature is higher than that during the afternoon at station *S* located in the Sendai Plain. This temperature difference should create the pressure difference that can generate the plain-to-basin wind. At station *S,* the wind direction changed to northeasterly at about 1300 JST, which is too late to be specified as a sea breeze. The direction also differs from the surface wind in other parts of the Sendai Plain where the sea breeze is southeasterly. At stations *S, Y,*

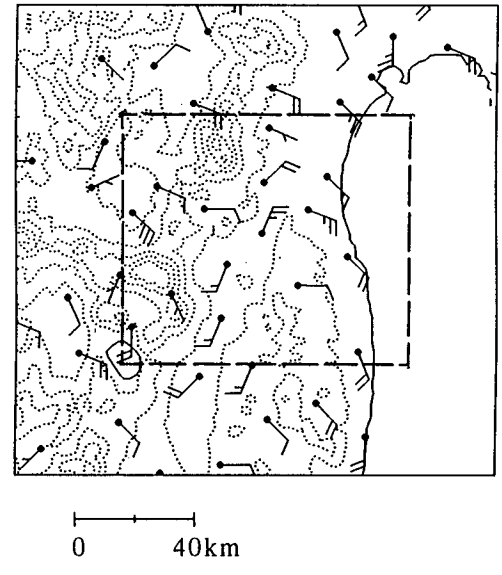

FIG. 16. The surface wind velocity observed in the vicinity of the Fukushima Basin at 1500 JST 8 June 1991, by the AMeDAS of the JMA. The box of broken lines indicates the area shown by Fig. 14.

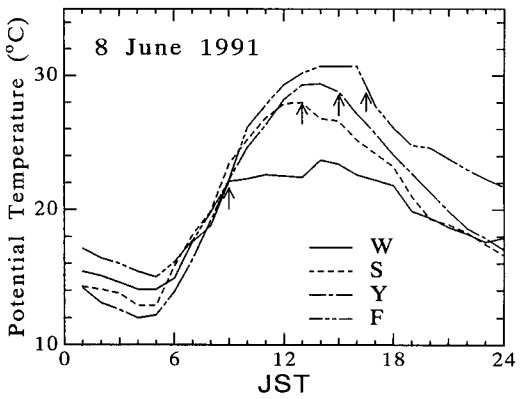

FIG. 17. The diurnal variation of surface temperature observed on 8 June 1991 at four stations indicated by *W, S, Y,* and *F* in Fig. 13. The arrows denote the time when the wind direction changed to southwesterly (station *W*) or northerly (stations *S, Y,* and *F*).

and *F* the temperatures began to decrease just after the wind direction changed to northerly.

6. Conclusions

The plain-to-basin wind is a thermally induced circulation that is generated as follows. During the daytime, upslope winds (valley winds) develop on each slope of the mountains surrounding the basin. These winds are composed of individual circulations, separate from the inside and outside of the basin. The atmospheric temperature in the boundary layer within the basin becomes higher than that outside, so that the surface pressure at the bottom of the basin is lower than that outside.

At dusk, the thermal forcing due to the surface heat flux decreases and the valley winds then weaken. The plain-to-basin wind develops over the mountain ridges and transports the cooler air from the outside mixed layer to inside the basin by passing over the ridges.

The plain-to-basin circulation is generated when the altitude of the mountain range is almost equal to or less than the maximum mixing height developed over the plain. Higher mountain ranges act as potential barriers of the circulation.

If a mountain pass exists with a lower elevation than the surrounding mountain range, the plain-to-basin circulation begins earlier in this region, since the upslope winds in the region that tend to block the circulation during the daytime are weak.

The plain-to-basin winds are most remarkable when the horizontal scale of the basin is less than approximately 100 km and the height of the mountain range is approximately equal to the maximum mixing height. For larger horizontal scales, the velocity of the plain-to-basin wind is weaker.

Plain-to-basin winds are observed in the Usui Pass and the northern Fukushima Basin in Japan. Since the elevation of Usui Pass is about 1 km, the plain-to-basin wind develops after sunset. In the northern Fukushima Basin, however, the plain-to-basin wind can be observed during the afternoon, because the altitude of the channellike valley connecting the basin and the plain is less than approximately 100 m.

Acknowledgments. The authors would like to thank Prof. J. Kondo of Tohoku University for helpful discussions and useful advice. The authors would also like to thank the staff and students of Tohoku University.

REFERENCES

Bhumralkar, C. N., 1975: Numerical experiments on the computation of ground surface temperature in an atmospheric general circulation model. *J. Appl. Meteor.*, **14,** 1246–1258.

Bougeault, P., 1983: A non-reflective upper boundary condition for limited-height hydrostatic models. *Mon. Wea. Rev.*, **111,** 420–429.

Kikuchi, Y., S. Arakawa, F. Kimura, K. Shirasaki, and Y. Nagano, 1981: Numerical study on the effects of on the land and sea breeze circulation in the Kanto District. *J. Meteor. Soc. Japan,* **59,** 723–738.

Kimura, F., and S. Arakawa, 1983: A numerical experiment of the nocturnal low level jet over the Kanto plain. *J. Meteor. Soc. Japan,* **61,** 848–861.

——, and T. Yoshikawa, 1988: Numerical simulation of global scale dispersion of radioactive pollutants from the accident at the Chernobyl Nuclear Power Plant. *J. Meteor. Soc. Japan.*, **66,** 489–495.

Klemp, J. B., and D. R. Durran, 1983: An upper boundary condition permitting internal gravity wave radiation in numerical mesoscale models. *Mon. Wea. Rev.*, **111,** 430–444.

Kondo, J., T. Kuwagata, and S. Haginoya, 1989: Heat budget analysis of nocturnal cooling and daytime heating in a basin, *J. Atmos. Sci.*, **46,** 2917–2933.

——, T. Nakamura, T. Yamazaki, 1990: Estimation of the solar and downward atmospheric radiation. *Tenki,* **38,** 42–48 (in Japanese).

Kurita, H., H. Ueda, and S. Mitusmoto, 1990: Combination of local wind systems under light gradient wind conditions and its contribution to the long-range transport of air pollutants. *J. Appl. Meteor.*, **29,** 331–348.

Kuwagata, T., and M. Sumioka, 1991: The daytime PBL heating process over complex terrain in central Japan under fair and calm weather conditions. Part III: Daytime thermal low and nocturnal thermal high. *J. Meteor. Soc. Japan,* **69,** 91–104.

——, ——, N. Masuko, and J. Kondo, 1990a: The daytime PBL heating process over complex terrain in central Japan under fair and calm weather conditions. Part I: Meso-scale circulation and the PBL heating rate. *J. Meteor. Soc. Japan,* **68,** 625–638.

——, ——, ——, and ——, 1990b: The daytime PBL heating process over complex terrain in central Japan under fair and calm weather conditions. Part II: Regional heat budget, convective boundary layer height and surface moisture availability. *J. Meteor. Soc. Japan,* **68,** 639–650.

Mellor, G. L., and T. Yamada, 1974: A hierarchy of turbulence closure models of planetary boundary layers. *J. Atmos. Sci.*, **31,** 1791–1805.

Whiteman, C. D., 1990: Observations of thermally developed wind system in mountainous terrain. *Atmospheric Processes over Complex Terrain,* W. Blumen, Ed., Amer. Meteor. Soc., 5–42.